Heat Mass Transfer (2018) 54:277–290
DOI 10.1007/s00231-017-2122-4

ORIGINAL

Experimental study on forced convective and subcooled flow boiling heat transfer coefficient of water-ethanol mixtures: an application in cooling of heat dissipative devices

B. G. Suhas[1] · **A. Sathyabhama**[1]

Received: 2 January 2017 / Accepted: 24 July 2017 / Published online: 1 August 2017

Abstract The experimental study is carried out to determine forced convective and subcooled flow boiling heat transfer coefficient in conventional rectangular channels. The fluid is passed through rectangular channels of 0.01 m depth, 0.01 m width, and 0.15 m length. The parameters varied are heat flux, mass flux, inlet temperature and volume fraction of ethanol. Forced convective heat transfer coefficient increases with increase in heat flux and mass flux, but effect of mass flux is less significant. Subcooled flow boiling heat transfer increases with increase in heat flux and mass flux, but the effect of heat flux is dominant. During the subcooled flow boiling region, the effect of mass flux will not influence the heat transfer. The strong Marangoni effect will increase the heat transfer coeffient for mixture with 25% ethanol volume fraction. The results obtained for subcooled flow boiling heat transfer coefficient of water are compared with available literature correlations. It is found that Liu-Winterton equation predicts the experimental results better when compared with that of other literature correlations. An empirical correlation for subcooled flow boiling heat transfer coefficient as a function of mixture wall super heat, mass flux, volume fractions and inlet temperature is developed from the experimental results.

Keywords Cold plate · Forced convection · Heat dissipative devices · Marangoni force · Rectangular channel

✉ B. G. Suhas
suhas_bg@yahoo.co.in

[1] Mechanical Engineering Department, National Institute of Technology, Karnataka, Srinivasanagara, Surathkal, Mangalore 575025, India

Nomenclature

B_o	Boiling number
C_p	Specific heat (kJ/kg-K)
D_h	Hydraulic diameter (m)
E	Enhancement factor
G	Mass flux (kg/m^2-s)
h	Heat transfer coefficient (kW/m^2-K)
h_{fg}	Latent heat of vaporization (kJ/kg)
k	Thermal conductivity (kW/m-K)
M	Molecular mass (kg/mol)
Nu	Nusselt number
P	Pressure (N/m^2)
Pr	Prandtl number
$q^{"}$	Heat flux (kW/m^2)
Re	Reynolds number
T	Temperature (K)
ΔT	Temperature difference (K)
v_f	Volume fraction of ethanol (%)
x	Vapour quality
X	Position (m)
z^*	Dimensionless distance for thermally developing flow

Greek letters

ρ	Density (kg/m^3)
μ	Dynamic viscosity (kg/m-s)
ω	Uncertainty
σ_s	Surface Tension (N/m)
χ_{tt}	Martinelli parameter

Subscript

b	Bubble point
cr	Critical
d	Dew point
f	Fluid
fc	Forced convection
fr	First row
g	Gaseous

i Independent parameter
l Liquid
in Inlet
pb Pool boiling
Sr Second row
tp Two phase
σ Standard deviation
W Wall

1 Introduction

The present day technology in the nuclear industries, petroleum refineries, chemical industries, process industries, automobile industries, refrigeration systems endeavor to meet the demand and supply in daily life of mankind. In these industries, heat is dissipated from the catalytic reactors, batteries, electronic devices, burners, radiators etc. The overheating affects the durability and performance of these devices. Therefore the primary concern is for cooling of these devices. Maintaining the peak temperature of the heat source below an allowable level is a major concern in the design of a cooling system. In some applications, heat flux is high enough to encounter subcooled boiling of the liquid. The complexities encountered in the boiling process have stimulated numerous investigators to conduct extensive research in this field [1]. Nowadays, determining the heat transfer coefficient in any power cycles or phase changing processes related to boiling operation is a key parameter in designing of cooling equipments [2, 3]. Because of the superior heat transfer rate as the result of phase change phenomenon, boiling has widely been used as a dominant heat transfer mechanism in heat dissipative devices [4–6]. Due to the complication of the boiling phenomena as well as unknown interactions between a numbers of sub processes, real facts about boiling are still unknown [7]. A nucleate boiling system is comprised of three main heat transfer mechanisms: (i) heat conduction through liquid from the boiling surface to the liquid–vapor equilibrium interface, (ii) evaporation at the liquid–vapor interface toward the vapor phase, (3) departing the vapor from the heating surface in form of bubble and vapor blanket depending on the applied heat flux [8]. Nucleate boiling is divided into two regimes like subcooled boiling region and saturated boiling region. Subcooled flow boiling heat transfer of liquids has been studied extensively due to its wide applications in different industries. Subcooled flow boiling has gained more and more attention where high heat removal rates are required, such as in emergency core cooling of water cooled nuclear reactors, first wall cooling of fusion reactors, and cooling of neutron accelerator targets [9]. Cooling by a fluid can be split into two categories, i.e., direct and indirect cooling. Direct cooling permits contact between the fluid and heat source. During indirect cooling a conductive thick plate is placed between the heat source and the flowing fluid as heat transfer interface. This a thermal pathway between heat source and the fluid. It is demonstrated that the thick plate can significantly improve the heat transfer between the heat source and the cooling fluid. This conductive plate is called as cold plate [10]. The fluid flow channels in the cold plate can be arranged according to different heat dissipation rate [11]. The cold plate configuration is classified into four major types as shown in Fig. 1:

a) Formed Tube Cold Plate (FTCP): The coolant tubes are inserted to the cold plate by soldering or using thermal epoxy. In this design, copper plate or aluminum plate is generally used. This kind of design is used for low heat flux application.
b) Deep Drilled Cold Plate (DDCP): In this design, deep holes are drilled in the plane of the plate, which are generally made of copper or aluminum. These holes are fitted with end caps (or plugs) to create coolant flow path through the plate. This kind of design is used for medium heat flux application.
c) Machined Channel Cold Plates (MCCP): In this design, the channels are machined in the base plate itself. Depending on the thermal performance desired, these channels can vary in width from 10 mm wide to 200 μm microchannels. This kind of design is used for high heat flux applications of above 100 W/cm^2. Hence this type of cold plate is used in the present study.
d) Pocketed Folded-Fin Cold Plates (PFFCP): The local heat transfer coefficient, as well as the surface area in the coolant passages, can be enhanced by introducing fins in the coolant channels. In this design recessed pockets are machined to various folded fin inserts and are soldered inside the passages. This kind of design is used for extremely high heat flux applications.

Three important performance measures are considered: temperature uniformity along the cold plate, mean wall temperature of the cold plate and pressure drop. The mean wall temperature of the cold plate is the most sensitive to the operating conditions, especially with respect to the distribution of the input heat flux, and also to the coolant flow rate. The role of the cold plate is to convert the unfavorable non uniform heat flux distribution at the lower surface of the plate. There are few designs available for channel path in the cold plates. They are serpentine shaped, single S configured and double S configured. These design lead to pressure drop of the coolant at higher flow rate. The thick plate with variable cross section area reveals no significant advantage in the literature. The efficiency of the optimized plate on minimizing the target peak temperature depends upon the Reynolds number of the fluid flow, Prandtl number and the material thermal conductivity only [12].

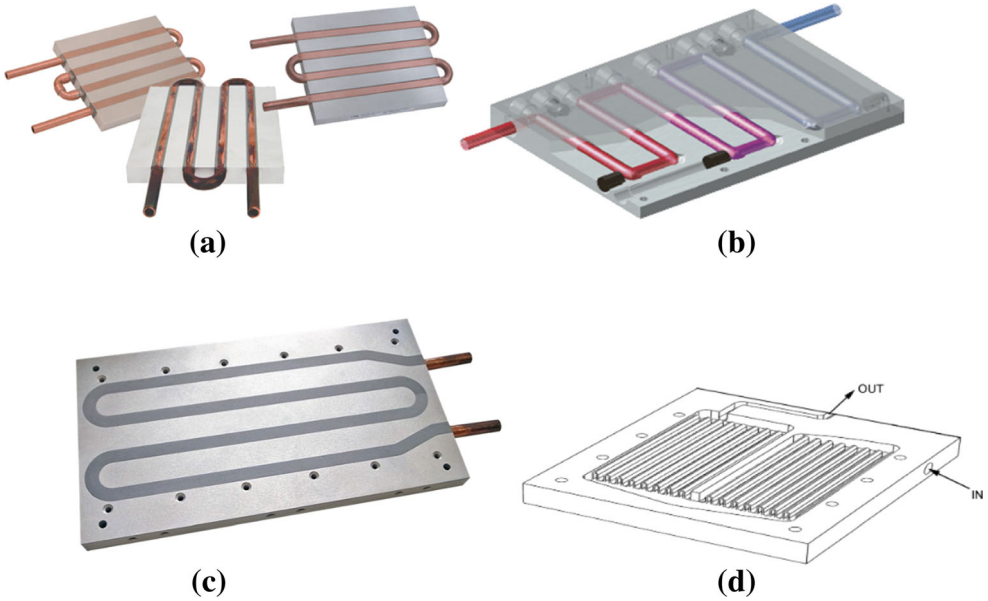

Fig. 1 **a** FTCP. **b** DDCP. **c** MCCP. **d** PFFCP (http://www.lytron.com/Cold-Plates)

The liquid which is used as coolant must meet certain requirements. The ozone depletion potential (ODP) and global warming potential (GWP) must be minimum for these coolants. The coolant must have high-dielectric strength. High-dielectric strength prevents current from travelling through the working fluid which cause damage or malfunction of battery component by short circuit. In the past decades, refrigerants were the fluids mainly used for cooling purposes. But the impact of these fluids on the environment has been identified in recent times. Therefore replacement of these liquids with similar heat transfer coefficients are necessary. The use of mixtures is one of the alternatives for the choice of a liquid that could be competent to the refrigerants. Miscellaneous binary mixtures are used as working fluids in studies in order to determine the potential increase in heat transfer comparing to their pure components or other pure liquids. Flow boiling of binary mixtures is more complicated than the corresponding pure fluids because (a) boiling point temperature varies with the mixture composition (b) thermo-physical properties of the mixture do not follow linear mixing laws (c) the overall transport mechanism is limited by the mass transfer process of the less volatile component during phase-change, and (d) the bulk liquid contact angle, which is important for understanding boiling mechanism, usually shows highly non-linear behavior with varying concentration. There is very limited availability of literature on flow boiling of binary mixtures, other than refrigerants, especially in conventional, mini and microchannels [13]. The binary mixture like water-glycol are expensive and require considerably higher pumping power due to their higher viscosity. Water-methanol is toxic in nature. For cost effectiveness and environmental concern water-ethanol mixture can be used in cooling the heat dissipative devices. The subcooled flow boiling of water-ethanol mixture is pertinent to the operation of heat dissipative devices like small catalytic reactors, electronic devices and HEV battery module.

Manoj et al. [14] conducted an experiment using water-ethanol mixtures in a 256 μm square channel. The heat transfer coefficient remained almost constant in the single-phase region and suddenly increased in the two-phase region. Heat transfer coefficient decreased at higher wall super heat. Chin et al. [15] conducted an experimental study on the convective boiling heat transfer of ethanol–water mixtures in a diverging microchannel with artificial cavities. The result showed that the boiling heat transfer was significantly influenced by the molar fraction as well as the mass flux. Suhas and Sathyabhama [16] conducted a numerical study on the single phase forced convective heat transfer of water-ethanol mixtures. It was found that increase in heat transfer coefficient was dependent more on Reynolds number than heat fluxes. But at higher ethanol mass fractions, the heat transfer coefficient increased when heat flux increased. An experimental investigation was conducted by Mark and Kandlikar [17] to study the single phase flow of degassed water in 207 mm hydraulic diameter of trapezoidal microchannels during laminar flow. The Nusselt numbers for their experimental data fell between the constant temperature and constant heat flux boundary conditions. Series of experiments on the boiling incipience were performed for water by Chang et al. [18]. The inception wall superheat was dependent on the inlet subcooling, heat flux and mass flux, but the variation of pressure did not lead to a significant change in boiling incipience. Sarfaraz et al. [19] studied subcooled nucleate flow boiling heat transfer of dilute water–diethylene glycol (DEG) mixtures inside a vertical annulus. Results revealed that increase in heat flux caused the single phase heat transfer coefficient to increase marginally till

the incipience of bubble formation. The flow boiling heat transfer coefficient increased when heat flux increased. Studies were carried out to design cold plate for cooling HEV battery modules. Anthony et al. [20] analysed the influence of different operating conditions such as heat flux and coolant mass flow rate on the cold plate with a single serpentine path having rectangular cross section channel for water-ethylene glycol mixture. Increase in mass flow rate of the coolant reduced the temperature of battery cells. A simulation work on lithium ion battery cells cooling for automotive application with de-ionized water as the coolant was carried by Inigo et al. [21]. The channel path was serpentine with circular cross section tube which was attached to a cold plate. It was determined that the internal temperature of the cells did not exceed the operating range specified by the manufacturer.

The heat transfer coefficient of water-ethanol mixture is required to design cooling equipments for the heat dissipative devices. There is a lack of knowledge with the basic mechanism associated with the subcooled flow boiling heat transfer phenomena of water-ethanol mixture. The understanding of the bubble behavior and its consequence on heat transfer is significant and contributes to a better understanding of physical phenomena in subcooled flow boiling of water-ethanol mixture. In the present research, subcooled flow boiling of water-ethanol mixture is pertinent to the operation of small catalytic reactors, electronic devices and HEV battery module. In present research, the experiment is conducted to determine the single phase forced convective and subcooled flow boiling heat transfer coefficients of water-ethanol mixture for various parameters like heat flux (from 21.78 kW/m^2 to 133.47 kW/m^2), mass flux from 76.67 kg/m^2-s to 228.33 kg/m^2-s), inlet temperature (303 K, 313 K and 323 K) and volume fraction of ethanol (0%, 25%, 50%, 75% and 100%).

2 Experimental methodology

2.1 Experimental setup and procedure

The schematic diagram of experimental test set up is shown in Fig. 2. The experimental test set up is a closed loop having rectangular aluminum block consisting of two rectangular channels, condenser coil dipped in ice water bath, reservoir, pump with variable flow rate and preheater. The aluminum block consisting of two channels of 10 mm (width) × 10 mm (height)× 150 mm (Length) is shown in Fig. 3. The aluminum block is considered as cold plate. Two cartridge heaters are inserted inside the cold plate. Heat loss is prevented by providing mineral wool as insulating material. The wall temperature, fluid inlet and outlet temperatures of the channel are also measured by thermocouples and are displayed in the indicator panel. The high speed camera is

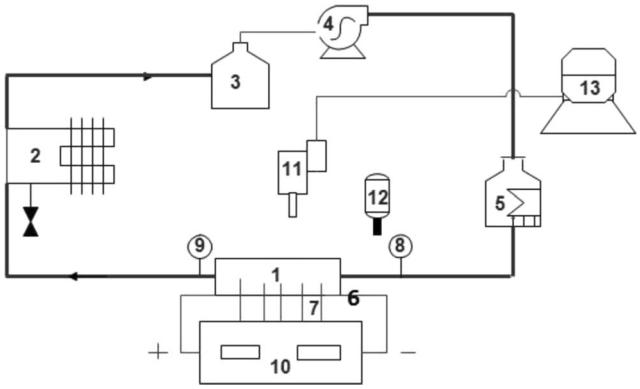

Fig. 2 Schematic diagram of experimental setup. (1) Rectangular aluminum block consisting of two rectangular channels. (2) Condenser coil dipped in ice water bath. (3) Reservoir. (4) Pump having variable flow rate. (5) Preheater. (6) Cartridge heaters. (7) Thermocouples to measure wall temperature. (8) Channel inlet fluid temperature measuring thermocouple. (9) Thermocouples to measure channel inlet and outlet fluid temperatures. (10) Temperature indicator panel (11) High speed camera. (12) Light source.(13) Data Aquisiation system for flow visualization

used for flow visualization. The equipment used in the present experiment is shown in Table 1. Figure 4 shows the arrangement of thermocouples in the cold plate to measure wall temperature and to calculate heat flux. The first set of five thermocouples (T_{11}, T_{12}, T_{13}, T_{14} and T_{15}) are placed 2 mm below the channel in a row. The second set of five thermocouples (T_{21}, T_{22}, T_{23}, T_{24} and T_{25}) are placed 20 mm below the first row of thermocouples. The distance between each thermocouple in a row is 25 mm. Two cylindrical cartridge heaters are placed 40 mm below the channels. The averages of five heat fluxes and wall temperature which are obtained from five different points in the channel are considered to calculate the heat transfer coefficient. It is observed that the heat flux value is higher at the inlet of the channel and decreases along the channel length. It is also observed that the wall temperature is lower at the entrance and marginally increases along the channel length. Due to the possibility of solubility of air in water and ethanol, degassing is done for around thirty minutes before commencing the experiment

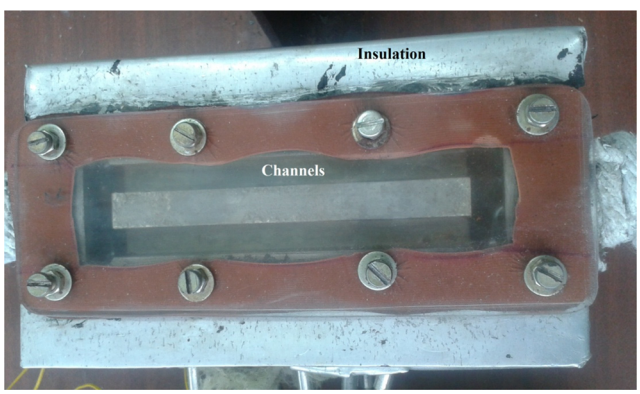

Fig. 3 Aluminum block with rectangular channels

Table 1 Equipment used in the present experiment

Equipment	Specifications
k-type thermocouples (12 no's)	Range:-20°C to 400°C, Sheath length: 20 mm, sheath diameter: 1.2 mm
Cartridge heater (2 no's)	Diameter: 12.7 mm, Length: 180 mm, capacity: 750 W
Peristaltic pump	Capacity: 100 l per hour, Operating pressure: Atmospheric
Preheater	Chamber capacity: 4 Liters, Heater capacity: 3 kW.

[22]. It is found that there is negligible pressure drop across these conventional channels due to low mass flow rate and higher dimensions.

2.2 Data reduction

Fourier law of heat conduction is applied to calculate the heat flux from the measured values of temperature gradient and known value of thermal conductivity.

$$q'' = -k\frac{dT}{dx} \tag{1}$$

The heat flux is calculated by Eq. (2) by substituting the values of thermal conductivity of aluminum, temperatures and the distance between the rows in Eq. (1).

$$q'' = -k\frac{(T_{sr}-T_{fr})}{(X_{sr}-X_{fr})} \tag{2}$$

The heat flux is assumed to be the same for the bottom wall of the channel as the first row, since it is very near to the first rows of thermocouples (i.e. 2 mm). Therefore the wall temperature is considered equal to that of first row. The heat transfer coefficient is calculated by Eq. (4) from the calculated values of heat flux, calculated values of wall temperatures and measured values of outlet temperature. The average of five readings of wall temperatures is calculated to determine the difference between the wall and outlet fluid temperature.

$$h = \frac{q''}{(T_w-T_f)} \tag{3}$$

2.3 Uncertainties

According to International Bureau of weights and measures (IBWM) and International organization of standards (ISO) random of independent variables may be calculated using root-sum-square (RSS) of standard deviation [23]:

$$\omega_i = \sqrt{\omega_{i,resolution}^2 + \omega_{i,conversion}^2 + \omega_{i,calibration}^2 + s_{2\sigma_i}^2} \tag{4}$$

After determining the uncertainty of independent variables, the uncertainties of calculated parameters are determined by McClintock and Kline method [24]:

$$\omega_{cp}^2 = \sum_{i=1}^{n}\left(\frac{\partial f}{\partial x_i}\right)^2 \omega_{x_i}^2 \tag{5}$$

2.3.1 Uncertainty in temperature measurement

The Thermocouples are calibrated against an insulated ice bath and boiling water. The temperature equation follows linear relation which is given as $T_{Actual} = aT_{measured} + b$. The constants (a and b) for temperature measurement corrections are shown in Table 2. After allowing the system to stabilize for a period of two hours in the ice bath, all measured temperature readings fluctuated within ±0.3 °C. The voltage resolution in the data logger at a 100mv range signal is 0.01mv, corresponding to ±0.1°C and conversion accuracy is less than ±0.02°C. The standard deviation is found to be ±0.15°C. Since, the different components of the uncertainty are independent variables, the combined uncertainty of the temperature measurements can be calculated as shown in Eq. (6)

$$\omega_T = \pm\sqrt{\omega_{T,resolution}^2 + \omega_{T,conversion}^2 + \omega_{T,calibration}^2 + S_{2\sigma_T}^2} \tag{6}$$

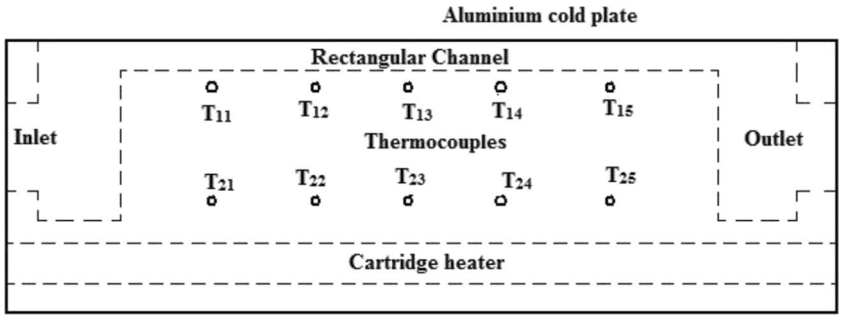

Fig. 4 Arrangement of thermocouples in the cold plate

Table 2 Temperature measurement corrections

Readings	Steam point (K)	Ice point (K)	a	b
T1	372	274	1.0204	−6.5896
T2	375	275	1	−2
T3	374	275	1.0101	−4.778
T4	375	275	1	−2
T5	374	273	0.990099	2.7029
T6	374	273	0.990099	2.7029
T7	373	274	1.0101	−3.7674
T8	375	274	0.9901	1.7129
T9	373	275	1.0204	−7.61
T10	373	274	1.0101	−3.7674
T11	372	273	1.0101	−2.75758
T12	371	275	1.04167	−13.458

2.3.2 Uncertainty in mass flux

The mass flux is the mass flow rate across unit area and is given by Eq. (7)

$$G = \frac{4m}{\pi {D_h}^2} \tag{7}$$

The uncertainty in mass flux is given by the uncertainty in liquid mass flow rate and uncertainty in channel dimensions.

$$\omega_G = \pm\sqrt{\left(\frac{\partial G}{\partial m}\omega_m\right)^2 + \left(\frac{\partial G}{\partial D_h}\omega_{D_h}\right)^2} \tag{8}$$

2.3.3 Uncertainty in heat flux

The uncertainty in heat flux is calculated by the independent variables like uncertainties in the temperature and distance measurements as given by Eq. (9)

$$\omega_{q''} = \pm\sqrt{\left(\frac{\partial q''}{\partial T_{wsr}}\omega_{T_{wsr}}\right)^2 + \left(\frac{\partial q''}{\partial T_{wfr}}\omega_{T_{wfr}}\right)^2 + \left(\frac{\partial q''}{\partial \Delta x}\omega_{\Delta x}\right)^2} \tag{9}$$

$\omega_{T_{wfr}}$ and $\omega_{T_{wfr}}$ are uncertainties in measuring wall temperatures in the first rows and seconds rows. $\omega_{\Delta x}$ is uncertainty in measuring distance between the first row and second row of thermocouples.

2.3.4 Uncertainty in heat transfer coefficient

The heat transfer coefficient is calculated from the uncertainty values of heat flux and temperature as given by Eq. (10)

$$\omega_h = \pm\sqrt{\left(\frac{\partial h}{\partial q}\omega_q\right)^2 + \left(\frac{\partial h}{\partial (T_w)}\omega_{T_w}\right)^2 + \left(\frac{\partial h}{\partial (T_f)}\omega_{T_f}\right)^2} \tag{10}$$

The uncertainties of independent and measured parameters is shown in Table 3.

3 Validation of experimental results obtained for water

Experimentally determined single phase forced convective heat transfer coefficient of water is used to calculate Nusselt number for validation purposes. The validation is carried for mass flux ranging from 76.67 kg/m^2-s to 228.33 kg/m^2-s, heat flux = 21.78–133.47 kW/m^2 and inlet temperature = 303 K–323 K. Mean absolute error (MAE) can be calculated by Eq. (11).

$$MAE = \frac{1}{n}\sum\frac{Thoretical\ values - Experimental\ values}{Theoretical\ values} \times 100 \tag{11}$$

Where, n refers to number of readings.

Nusselt number in a rectangular channel for single-phase flow can be calculated by the Churchill and Ozoe equation. Churchill and Ozoe equation was developed in terms of $Pr \to 0$ behavior and $Pr \to \infty$. The characteristics of this region for uniform wall temperature boundary condition are given as:

$$Pr \to 0 \quad \frac{Nu}{\sqrt{Re}} = 0.564 Pr^{0.5} \tag{12}$$

$$Pr \to \infty \quad \frac{Nu}{\sqrt{Re}} = 0.339 Pr^{0.33} \tag{13}$$

$$Nu = \frac{C_0\sqrt{RePr}}{\left[1 + \left(\frac{C_0 \mathrm{Pr}^{1/6}}{C_\infty}\right)^n\right]^{1/n}} \tag{14}$$

C_0 and C_∞ are the coefficients of the right hand side of Eqs. (13) and (14) and n = 4.598 for the uniform temperature boundary condition [25]. For a parallel rectangular channel,

Table 3 Uncertainties of measured and calculated parameters

Parameters	Uncertainties
Thermocouple	±0.35°C (RSS)/±0.1°C (resolution)
Preheater temperature	±0.1°C (resolution)
Mass flow rate	±2.32%
Mass flux	±0.77%
Heat flux	±13.3%
Heat transfer coefficient	±9.11%

Stephan correlated numerical results for Nusselt number as shown in Eq. (15). This equation is valid for Prandtl numbers varying from 0.1 to 1000 and for laminar flows [26].

$$Nu = 7.55 + \frac{0.024(z^*)^{-1.14}}{1 + 0.035\mathrm{Pr}^{0.17} z^{*-0.64}} \tag{15}$$

The theoretical values calculated from correlation under predicted the experimental values as shown in Figs. 5 and 6. Following are the observations made from validation.

- 63% of experimental data are predicted within ±20% error band and 26.15% experimental data are predicted within error band of ±10%. The MAE of experimental data while predicting with Churchill-Ozoe correlation is 19.78%.
- 81.54% of experimental data lie within ±30% error band and 61.54% of experimental data lie within error band of ±20%. The MAE of experimental data while predicting with Stephan correlation is 21.55%.

Chen [27] redeveloped the Rohsenow correlation for subcooled boiling heat transfer coefficient:

$$h_{tp} = Fh_{fc} + Sh_{pb} \tag{16}$$

$$h_{fc} = 0.023Re^{0.8}Pr^{0.4}\frac{k_l}{D_h} \tag{17}$$

$$h_{pb} = 0.00122\frac{k^{0.79}C_P^{0.45}\rho_l^{0.49}}{\sigma^{0.5}\mu_l^{0.29}h_{fg}^{0.24}\rho_g^{0.24}}\Delta T_{Sat}^{0.24}\Delta p_{Sat}^{0.75} \tag{18}$$

$$F = \left(1 + \frac{1}{(\chi_{tt})^{0.5}}\right)^{1.78} \tag{19}$$

$$\chi_{tt} = \left(\frac{1-x}{x}\right)^{0.9}\left(\frac{\rho_g}{\rho_l}\right)\left(\frac{\mu_l}{\mu_g}\right)^{0.1} \tag{20}$$

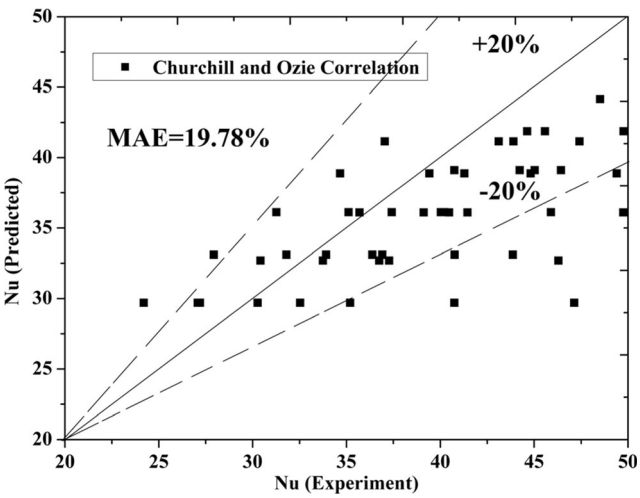

Fig. 5 Validation of forced convective heat transfer coefficient values with Churchill and Ozoe correlations

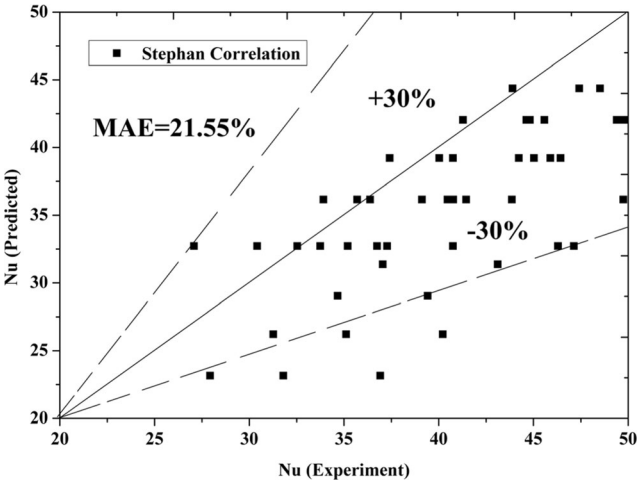

Fig. 6 Validation of forced convective heat transfer coefficient values with Stephan correlation

$$S = \frac{1}{1 + 2.53 \times 10^{-6}Re^{1.17}} \tag{21}$$

The Reynolds number factor F and the suppression factor S were determined empirically from experimental data [28]. Figure 7 shows that 81.5% of present experimental data are predicted within ±35% error band and 66.15% are predicted within error band of ±20%. The MAE of experimentally determined Nusselt number for water and those predicted with Chen correlation is 26.29%. The Chen correlation was developed by considering 600 data points for water and five organic fluids. The parameter range were vapour quality from 0.01 to 0.71, mass flux from 54 to 4070 kg/m^2-s, heat flux from 6.3 to 2397.5 kW/m^2, and saturation pressure from 0.055 to 3.48 MPa. The other reason for deviation is the presence of Reynolds number factor F in the Chen correlation. F is a function of Martinelli parmeter (χ_{tt}) as shown in Eq. (20).

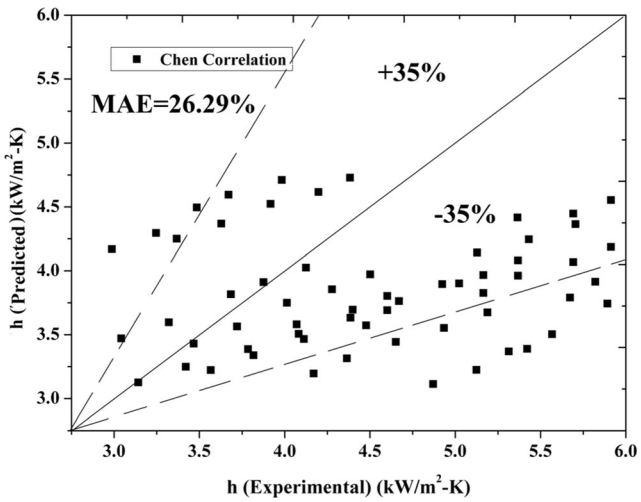

Fig. 7 Validation of subcooled flow boiling heat transfer coeffcient values with Chen correlation

Martinelli parameter is determined from vapour quality. Since the presence of vapour quality is negligible during the subcooled boiling, F is chosen as 1 in the present experiment. Gungor - Winterton [29] modified the Chen correlation by introducing the dependence on the boiling number (Bo) in the enhancement factor E. They suggested Cooper correlation for pool boiling heat transfer component in the Eq. (22)

$$h_{pb} = 55\left(\frac{P}{P_{cr}}\right)^{0.12}\left[-log_{10}\left(\frac{P}{P_{cr}}\right)\right]^{-0.55} M^{-0.5} q''^{0.67} \quad (22)$$

$$S = \frac{1}{1 + 1.15 \times 10^{-6} E^2 Re^{1.17}} \quad (23)$$

$$E = 1 + 24000 Bo^{1.16} \quad (24)$$

h_{tp} and h_{fc} are calculated by Eqs. (17) and (18) respectively. Figure 8 shows that 78.64% of present experimental data are predicted within ±20% error band and 44.62% are predicted within ±10% error band. The MAE of experimentally determined Nusselt number for water and those predicted with Gungour -Winterton correlation is 16.83%. The Boiling number in Eq. (25) leads to relatively lower deviation when compared with that of Chen correlation. The Gungor and Winterton correlation was developed for 4300 data points for water, R11, R12, R113, R114 and Ethylene Glycol for various tube diameters, orientation of flow, mass flux, heat flux, saturation pressure and vapour quality. This is the reason for deviation of the present experimental data from those data predicted from the correlation. Kandlikar [30] proposed subcooled boiling correlations for water and is given by Eq. (25):

$$\frac{h_{tp}}{h_{fc}} = 1058 Bo^{0.7} F \quad (25)$$

h_{fc} is calculated by the Eq. (17). Figure 9 shows that 90.76% of experimental data are predicted within ±30% error band and which 75.92% of experimental data are predicted within ±20% error band. The MAE of experimentally determined Nusselt number for water and those predicted with Kandlikar correlation is 18.78%. Liu -Winterton [31] proposed a power-type addition model for the prediction of subcooled flow boiling heat transfer. The correlation for subcooled flow boiling heat transfer coefficient is expressed as:

$$h_{tp} = \sqrt{F h_{fc}^2 + \left(S h_{pb} \frac{T_{Wall} - T_{Sat}}{T_{Wall} - T_{Sat}}\right)^2} \quad (26)$$

$$S = \frac{1}{1 + 0.0055 F^{0.1} Re_l^{0.16}} \quad (27)$$

h_{pb} is calculated by Eq. (22). Figure 10 shows that 69.23% of present experimental data are predicted within ±20% error band and 38.46% are predicted within error band of ±10%. The MAE of Liu and Winterton correlation is 22.69% while predicting the experimental data. Their experiments were carried out in tubes and annuli and covered a range of mass flux from 12.4 to 8180 kg/m^2-s, Pressure from 0.05 to 20 MPa, and T_{sub} from 0 to 173 °C.

It can be seen that the Gungour-Winterton and Kandlikar correlations predicted the experimental data better when compared with that of Chen and Liu-Winterton correlations. This may be due to the presence of Boiling number in Gungour-Winterton and Kandlikar correlations. The boiling number plays a vital role during subcooled flow boiling heat transfer and it also proved to be significant while predicting the subcooled flow boiling heat transfer coefficient by heat transfer approach [32]. Boiling number is defined as the ratio of heat flux to heat of evaporation. When heat flux increases, the active nucleation sites increase. Isolated bubbles are formed

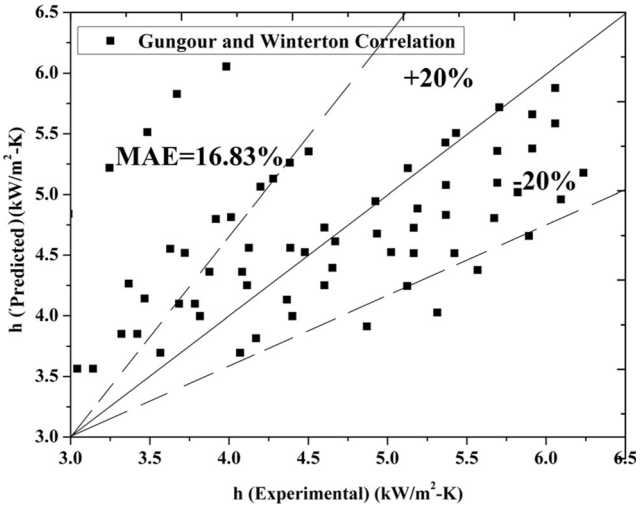

Fig. 8 Validation of subcooled flow boiling heat transfer coefficient values with Gungour and Winterton correlation

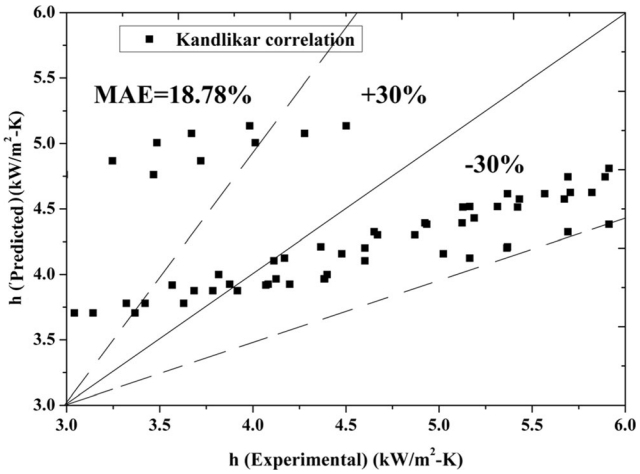

Fig. 9 Validation of subcooled flow boiling heat transfer coefficient values with Kandlikar correlation

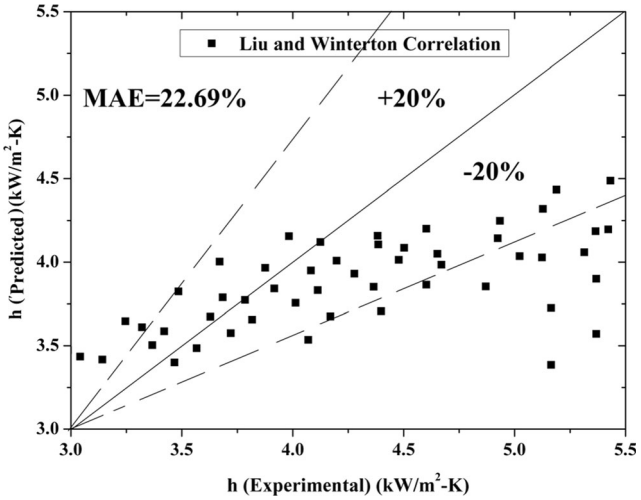

Fig. 10 Validation of subcooled flow boiling heat transfer coefficient values with Liu and Winterton correlation

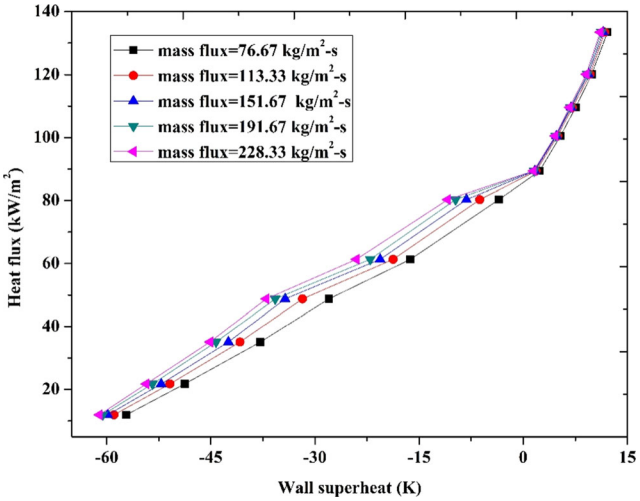

Fig. 11 Boiling curves for water at inlet temperature = 303 K

on active nucleation sites during nucleate boiling. After bubble inception, the superheated liquid layer which is pushed outward mixes with the subcooled liquid leading to agitation. The heat flux is considered by combining the effect of transient conduction around nucleation sites and micro-layer evaporation below the bubbles. The departed bubble acts as an energy carrier by removing the heat from the channel wall surface. Hence Boiling number is more significant in the subcooled boiling region. The deviation of the present experimental data from those predicted using correlations is also attributed to non-uniform temperature distribution in cold plate, assumption of one dimensional temperature distribution to calculate heat flux and non possibility of making the experimental system air tight.

4 Results and discussions

The experiments are conducted for various values of heat flux, mass flux, inlet temperature and concentration. About 550 experimental runs were carried out in the present study. These include 140 data for pure water 330 data for three different compositions of binary mixtures, and 80 data for pure ethanol. The heat transfer coefficient is calculated for various values of heat flux, mass flux, various inlet temperatures and volume fractions of ethanol.

4.1 Boiling curve

The variation of heat flux with wall superheat for water at inlet temperature = 303 K is shown in Fig. 11. The heat flux increases with increase in wall superheat for both single phase forced convection and subcooled boiling region. But the increase in heat flux is higher at subcooled boiling region. The boiling curves closely merge into a single curve for different values of mass fluxes. The increase in mass flux decreases the wall temperature in single phase forced convection region but the wall superheat do not vary significantly due to increase in mass flux at subcooled boiling regions. Decrease in wall temperature decreases the wall superheat. This shows that increase in mass flux has negligible influence on heat transfer in this region. During the onset of nucleate boiling (ONB), the bubble formation commences. The active nucleation sites occur due to micro layer evaporation in the corner of bottom wall of the channel. However, flow in the middle portion of the channel is subcooled. At higher heat flux, the buoyancy and inertial forces are significant than surface tension forces. The bubbles detach and depart from the corner and enter the subcooled region. With further increase in heat flux, the vapour generation commences, i.e., onset of vapour generation (OSV). This region is highly subcooled region. This results in the flow of surrounding fluid into the activation sites. This causes vapour turbulence and agitation, which causes the heat flux contribution towards the subcooled boiling heat transfer and significant over the forced convective heat transfer.

At higher heat fluxes, as the mass flux increases, the decrease in wall temperature is less due to decrease in subcooling of the fluid in the middle portion of the channel. The decrease in subcooling may due to i) diffusion of the bubbles which departed from corners and ii) formation of new nucleation sites at the bottom wall of the channel. Similar trends are observed for various values of ethanol volume fractions and inlet temperatures.

4.2 Effect of heat flux and mass flux

Figure 12 shows the variation of heat transfer coefficient of water with different wall super heats for varying mass fluxes. In this Figure the wall superheat is the function of heat flux. The heat transfer coefficient increases with increase in heat flux and mass flux for both the regions. Heat transfer

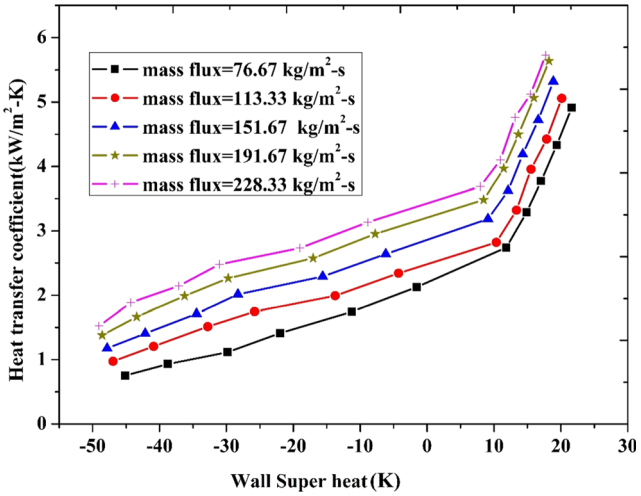

Fig. 12 Variation of heat transfer coefficient of water with wall super heat for various mass fluxes at inlet temperature = 303 K

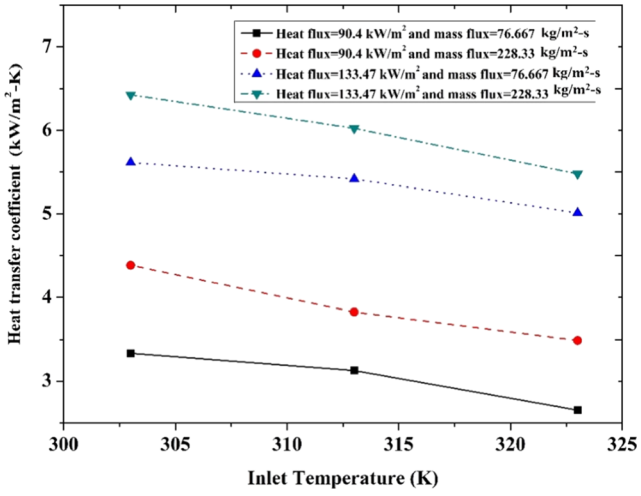

Fig. 13 Variation of forced convective heat transfer coefficient of water with inlet temperatures

coefficient increases with decrease in fluid temperature and wall temperature. This is observed in both the regions. In the subcooled boiling region, decrease in wall temperature with an increase in mass flux is insignificant. During the commencement of ONB, bubbly flow occurs. In bubbly flow, the liquid micro layer film is formed due to evaporation. The bubbly flow also continues in highly subcooled OSV region. The micro layer acts as blanket and thus preventing the large decrease in wall temperature. The heat transfer coefficient increases with increase in heat flux in the forced convection region. But the increase is not significant, as by the time of increase in heat transfer, the higher velocity of the liquid will carry away the heat which is conducted to the channel. The effect of mass flux is not significant to increase heat transfer coefficient in subcooled boiling region. This is because convective contribution does not play a significant role on the heat transfer due to establishment of vapour turbulent flow. Higher mass flux contributes towards convective mode of heat transfer, but the convective heat transfer is dominated by vapour turbulence in the flow. The vapour bubble is subjected to variation of surface tension force, thus drags the adjacent warm layer of fluid and causing the flow around the bubble from hot region to cold region. This causes local vapour momentum forces acting in the flow. These local vapour momentum forces dominate the convective mode of heat transfer to increase the heat transfer coefficient.

4.3 Effect of inlet temperature

Figure 13 shows the variation of forced convective heat transfer coefficient for different inlet temperatures of water. It is observed that the forced convective heat transfer coefficient decreases with an increase in inlet temperature. This may be because of increase in thermal boundary layer thickness at the entry of the channel. Higher the thickness, lower is the potential to absorb heat. Figure 14 shows the variation of subcooled boiling heat transfer coefficient with different inlet temperatures of water. This is also attributed to increase in thermal boundary layer like forced convective flow. Increase in inlet temperature also causes lesser bubble formation, thus reducing the vapour turbulence and vapour momentum forces. Hence the vapour bubble agitation and heat transfer decreases with increase in inlet temperature.

4.4 Effect of ethanol volume fraction

Figure 15 shows the variation of single phase forced convective heat transfer coefficient with volume fractions at various inlet temperatures. The ethanol-water mixture has a positive deviation from Raoult's law. This may result in decrease of surface tension with increase in ethanol volume fraction at single phase forced convective region. Addition of ethanol

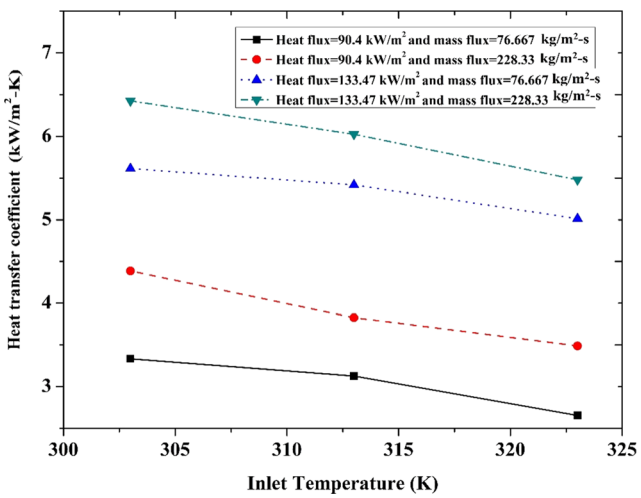

Fig. 14 Variation of subcooled boiling heat transfer coefficient of water with inlet temperatures

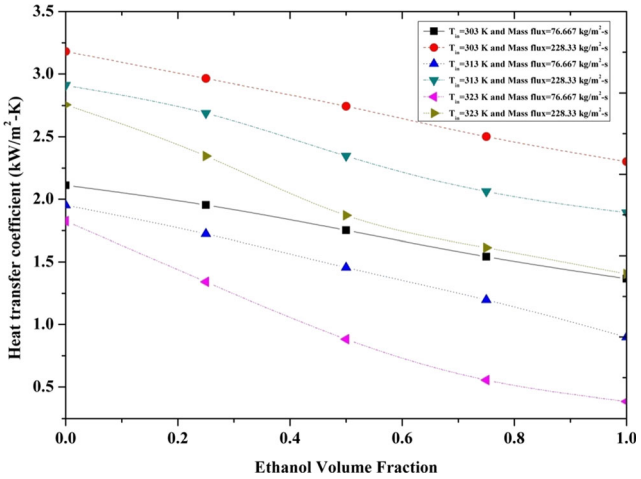

Fig. 15 Variation of forced convective heat transfer coefficient with ethnaol volume fraction for various mass fluxes and inlet temperatures

also decreases the thermal capacity and thermal conductivity which decreases the heat transfer coefficient.

Figure 16 shows the variation of subcooled flow boiling heat transfer coefficient with ethanol volume fraction for various inlet temperatures and constant heat flux = 90.4 kW/m^2. Similar trends are observed for both the cases. This particular value of heat flux is so chosen that the subcooled boiling takes place for both water and ethanol. If the heat flux is lower than 90.4 kW/m^2, subcooled boiling of water will not commence, instead it will be in forced convective region. If the heat flux is higher than 90.4 kW/m^2, saturated boiling of ethanol will be initiated. It is observed that the heat transfer coefficient increases for mixture with 25% ethanol volume fraction. The heat transfer coefficient further decreases for mixtures with 50% and 75% ethanol volume fraction and increases for pure ethanol. At higher heat flux, heat transfer coefficient increases due to early bubble departure and formation of more number of active nucleation sites, i.e. bubble formation. Therefore, effect of increase in heat flux on heat transfer coefficient is more significant when compared with that of mass flux. But at higher mass flux, the bubble departs at earlier stage and active nucleation site formation is reduced due to decrease in wall temperature. At 25% volume fraction, maximum difference between dew point temperature and bubble point temperature is observed as shown in Fig. 17. The maximum difference between dew point and bubble point temperatures indicates that the liquid vapour coexisting region is widest at 25% ethanol volume fraction. During the onset of boiling more volatile component of the mixture near the channel wall surface induces concentration and temperature gradients in the micro layer region along the vapour-liquid interface. The induced gradients cause the Marangoni force to pull the bulk liquid towards the liquid vapour interface causing micro layer agitation and thus increasing the heat transfer coefficient.

The components in the liquid mixture have different evaporation rates. The lower boiling component escapes from the liquid-vapor interface and the higher boiling component accumulates near the liquid-vapor interface. The layer of the concentration gradient forms near the interface. Because of two phase and convective heat transfer, the concentration gradient layer exists not only at the surface of the bubble but also at the liquid - vapor interface at the bottom wall. Mass diffusion which exists during the convective heat transfer process affects the heat transfer coefficient of mixture during the subcooled flow boiling process. The lower boiling component in the liquid bulk has to pass through the diffusion layer before arriving at the interface. Therefore, for a mixture, the heat transfer coefficients are affected not only by the interaction between the two phase flow and the convective heat transfer, but also by the mass transfer resistance inside the diffusion layer [33]. The concentration gradient near the interface of evaporation is low because the evaporating process is less vigorous. Moreover, a bubble transitioning from the liquid to

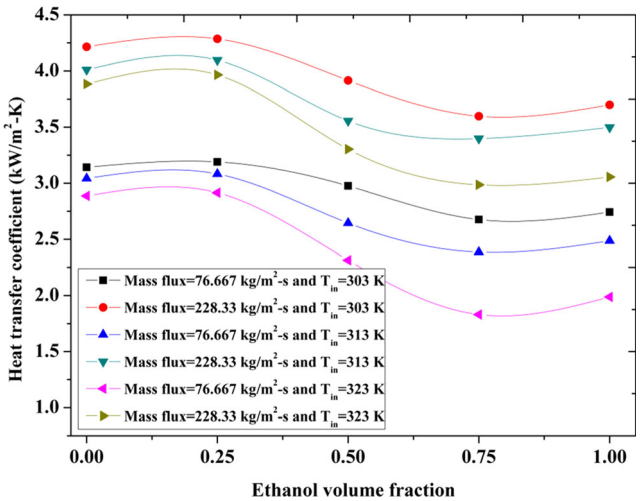

Fig. 16 Variation of subcooled boiling heat transfer coefficient with ethnaol volume fraction at various inlet temperatures

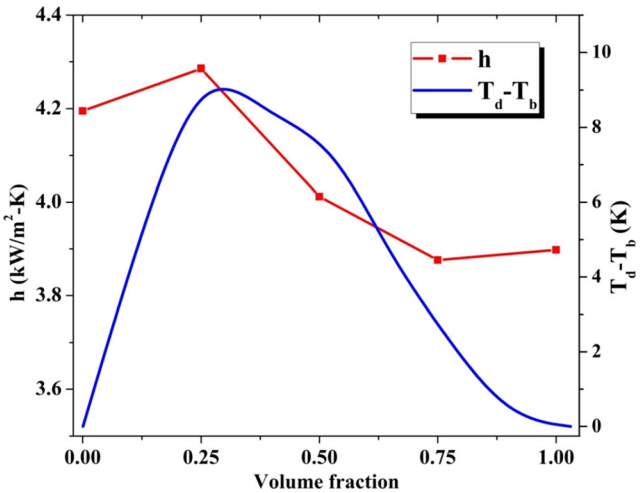

Fig. 17 Variation of heat transfer coefficient and $(T_d - T_b)$ with volume fraction

the vapor phase can cause agitation that decreases the effect of the mass diffusion [34]. The mixture has lower heat transfer coefficient than that of pure component due to the presence of local vapour of lower boiling component in the mixture [35]. Therefore, the ethanol is having higher heat transfer coefficient than that of mixture with 75% ethanol volume fraction as shown in Fig. 17. The mixture with 25% ethanol volume fraction is having highest heat transfer coeffient when compared with the other ethanol volume fractions [36, 37]. Hence the addition of ethanol to water delays the departure of bubbles, thus decreasing heat transfer coefficient from the site causing an increase in bubble departure diameter. Therefore increase active nucleation sites at 25% ethanol volume fraction increases and decreases for 75% ethanol volume fraction as shown in Fig. 18a–e.

4.5 Correlation development

An empirical correlation based on the present experimental data is developed. Empirical Eq. (28) proposed is a function of experimental parameters like G, T_{in}, $\Delta T_{s,m}$, $q^{"}$ *and* v_f. Mathematical regression analysis is adopted to develop the correlation. This analysis develops the relation between the independent parameter and several other dependent parameters.

$$h_{exp} = \frac{378.15 G^{0.048} q^{0.247} \Delta T_{s,m}{}^{0.106}}{T_{in}^{0.145} v_f^{0.056}} \tag{28}$$

The developed empirical correlation is validated with the present experimental data as shown in Fig. 19. 84.24% of experimental data are predicted within ±25% error band and 39.29% of experimental data are predicted within error band of ±10%. The MAE of empirical correlation while predicting the present experimental data is 14.68%.

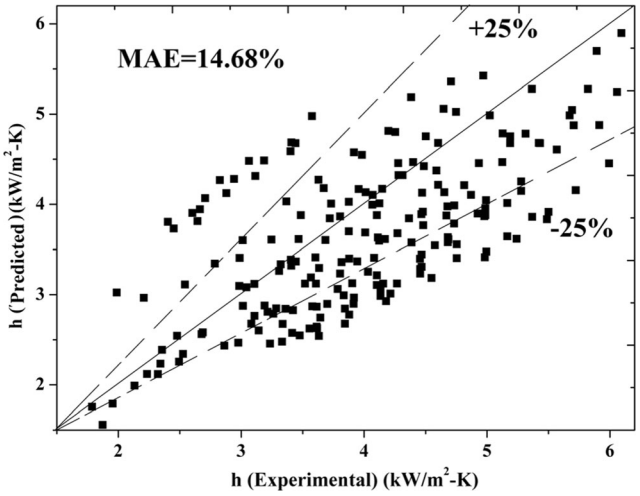

Fig. 19 Comparison of the experimental heat transfer coefficient with those predicted from the present correlation

5 Conclusions

The heat transfer coefficient of water-ethanol mixtures is determined for various values of heat fluxes, mass fluxes, inlet temperatures and ethanol volume fractions. The following conclusions are made from the experimental results.

- Forced convective heat transfer coefficient increases with an increase in heat flux and mass flux, but the effect of

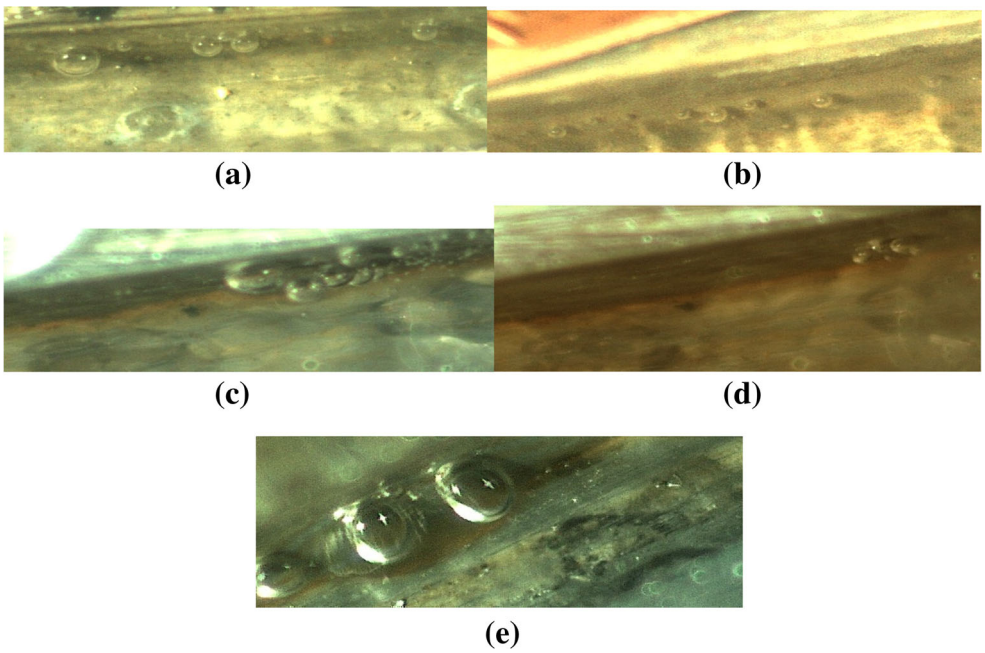

Fig. 18 Bubble formation at heat flux = 90.4 kW/m^2, inlet temperature = 303 K and mass flux = 76.67 kW/m^2. **a** water **b** 25% ethanol volume fraction **c** 50% ethanol volume fraction **d** 75% ethanol volume fraction **e** ethanol

heat flux was less significant. This is observed for all ethanol volume fractions.

- The MAE of experimental data while predicting with Churchill and Ozoe correlation and Stephan correlation are 19.78% and 21.55% respectively.
- Forced convective heat transfer coefficient of water decreases with addition of ethanol.
- Subcooled flow boiling heat transfer coefficient increases with an increase in heat flux and mass flux, but the effect of heat flux was more dominant. Increase in inlet temperature decreases the heat transfer coefficient in both the regions.
- The MAE of experimental data while predicting with Chen correlation, Gungour- Winterton correlation, Kandlikar correlation and Liu-Winterton correlation are 26.29%, 16.83%, 18.78% and 22.69% respectively.
- At 25% ethanol volume fraction, values of subcooled flow boiling heat transfer coefficient are higher at all values of mass flux and inlet temperatures. This is due to the presence of strong Marangoni forces.
- At 50% volume fraction subcooled boiling heat transfer coefficient is lower than that of 25% ethanol volume fraction and it further decreases at 75% ethanol volume fraction.
- The pure ethanol has higher subcooled flow boiling heat transfer coefficient than that of 75% ethanol volume fraction.
- 84.24% of experimental data are predicted within ±25% error band and 39.29% of experimental data are predicted within error band of ±10%. The MAE of empirical correlation while predicting the present experimental data is 14.68%.

References

1. Sarafraz MM, Peyghambarzadeh SM (2012) Experimental study on subcooled flow boiling heat transfer to water-diethylene glycol mixtures as a coolant inside a vertical annulus. Exp Thermal Fluid Sci 50:154–162
2. Sarafraz MM, Alavi Fazel SA, Hasanzadeh Y, Shamsabadi A, Bahram S (2012) Development of a new correlation for estimating pool boiling heat transfer coefficient of MEG/DEG/water ternary mixture. Chem Ind Chem Eng Q 18:11–18
3. Sarafraz MM, Alavi Fazel SA, Peyghambarzadeh SM, Vaeli N (2013) Nucleate pool boiling heat transfer of binary nano mixtures under atmospheric pressure around a smooth horizontal cylinder. Period Polytech, Chem Eng 57:71
4. Sarafraz MM, Hormozi F (2016) Experimental investigation on the pool boiling heat transfer to aqueous multi-walled carbon nanotube nanofluids on the micro-finned surfaces. Int J Therm Sci 100:255–266
5. Alavi Fazel SA, Sarafraz MM, Shamsabadi A, Peyghambarzadeh SM (2013) Pool boiling heat transfer in diluted water/glycerol binary solutions. Heat Transfer Eng 34:828–837
6. Sarafraz MM (2013) Experimental investigation on pool boiling heat transfer to formic acid, propanol and 2-butanol pure liquids under the atmospheric pressure. J Appl Fluid Mech 6:73–79
7. Sarafraz MM, Kiani T, Hormozi F (2016) Critical heat flux and pool boiling heat transfer analysis of synthesized zirconia aqueous nanofluids. Int Commun Heat Mass Transfer 70:75–83
8. Peyghambarzadeh SM, Sarafraz MM, Vaeli N, Ameri E, Vatani A, Jamialahmadi M (2013) Forced convective and subcooled flow boiling heat transfer to pure water and n-heptane in an annular heat exchanger. Ann Nucl Energy 53:401–410
9. Sarafraz MM, Peyghambarzadeh SM, Alavi Fazel SA (2012) Experimental studies on nucleate pool boiling heat transfer to ethanol/MEG/DEG ternary mixture as a new coolant. Chem Ind Chem Eng Q 8:577–586
10. Hajmohammadi MR, Salimpour MR, Saber M, Campo A (2013) Detailed analysis for the cooling performance enhancement of a heat source under a thick plate. Energy Convers Manag 76:91–700
11. Kandlikar SG, Hayner CN (2009) Liquid cooled cold plates for industrial high-power electronic devices—thermal design and manufacturing considerations. Heat Transfer Eng 30:918–930
12. Jarrett A, Ji YK (2011) Design optimization of electric vehicle battery cooling plates for thermal performance. J Power Sources 196:10359–10368
13. Cheng L, Mewes D (2006) Review of two-phase flow and flow boiling of mixtures in small and mini channels. Int J Multiphase Flow 32:183–207
14. Moharana MK, Rohan M, Nemad E, Khandekar S (2013) Phase-change heat transfer of ethanol-water mixtures: towards development of a distributed hydrogen generator, Proceedings of the ASME Summer Heat Transfer Conference, HT-2013, July 14–19, Minneapolis, Minnesota, USA
15. Fu BR, Tsou MS, Pan C (2012) Boiling heat transfer and critical heat flux of ethanol–water mixtures flowing through a diverging microchannel with artificial cavities. Int J Heat Mass Transf 55: 1807–1814
16. Suhas BG, Sathyabhama A (2016) Numerical analyses of single-phase pressure drop and forced convective heat transfer coefficient of water–ethanol mixture: an application in cooling of HEV battery module. Heat Transfer Asian Res 45(7):680–698
17. Steinke ME, Kandlikar SG (2004) An experimental investigation of flow boiling characteristics of water in parallel microchannels. J Heat Transf 126:518–526
18. Wang C, Wang H, Wang S, Gao P (2014) Experimental study of boiling incipience in vertical narrow rectangular channel. Ann Nucl Energy 66:152–160
19. Sarafraz MM, Peyghambarzadeh SM, Vaeli N (2012) Subcooled flow boiling heat transfer of ethanol aqueous solutions in vertical annulus space. Chem Ind Chem Eng Q 18(2):315–327
20. Anthony J, Li YK (2014) Influence of operating conditions on the optimum design of electric vehicle battery cooling plates. J Power Sources 245:644–655
21. Inigo A, Unai F, Jose A, Javier S, Ekaitz Z (2013) Li-Ion batteries for automotive applications. Congress on Numerical Methods in Engineering. June 25–28, Bilbao
22. Suhas BG, Sathyabhama A (2013) Bubble dynamics of water-ethanol mixture during subcooled flow boiling in a conventional channel. Appl Therm Eng 113:1594–1608. doi:10.1016/j.applthermaleng.2016.11.126
23. Kline SJ, McClintock FA (1953) Describing uncertainties in single-sample experiments. Mech Eng 75:3–8
24. Callizo CM (2010) Flow boiling heat transfer in single channel vertical diameter of small diameter, Doctoral Thesis, Department of energy technology, Royal Institute of Technology, Stockholm, Sweden, p 47–49
25. Churchill SW, Ozoe H (1973) Correlations for laminar forced convection in flow over an isothermal flat plate and in developing and

fully developed flow in an isothermal tube. ASME J Heat Transfer 95:416–419
26. Muzychka YS, Yovanovich MM (2002) Laminar flow friction and heat transfer in non-circular ducts and channels: part II—thermal problem. In: Celata GP, Thonon B, Bontemps A, Kandlikar S (eds) Compact heat exchangers: a Festschrift on the 60th Birthday of Ramesh K. Shah. Grenoble, France, August 24, 2002, p 131–139
27. Chen JC (1966) A correlation for boiling heat transfer to saturated fluids in convective flow. Ind Eng Chem Process Des Dev 5(3): 322–329
28. Chen W, Fang X (2014) A note on the Chen correlation of saturated flow boiling heat transfer. J Refrig 48:100–104
29. Gungor KE, Winterton RHS (1986) A general correlation for flow boiling in tubes and annuli. Int J Heat Mass Transf 29(3):351–358
30. Kandlikar SG (1998) Heat transfer characteristics in partial boiling, fully developed boiling. J Heat Transf 120:395–401
31. Liu Z, Winterton RHS (1991) A general correlation for saturated and subcooled flow boiling in tubes and annuli, based on a nucleate pool boiling equation. Int J Heat Mass Transf 34:2759–2766
32. Suhas BG, Sathyabhama A Heat transfer and force balance approaches in bubble dynamic study during subcooled flow boiling of water–ethanol mixture. Exp Heat Transfer. doi:10.1080/08916152.2017.1328469 (Available online)
33. Li M, Dang C, Hihara E (2012) Flow boiling heat transfer of HFO1234yf and R32 refrigerant mixtures in a smooth horizontal tube: Part I. Experimental investigation. Int J Heat Mass Transf 55: 3437–3446
34. Li M, Dang C, Hihara E (2013) Flow boiling heat transfer of HFO1234yf and R32 refrigerant mixtures in a smooth horizontal tube: Part II. Prediction method. Int J Heat Mass Transf 64: 591–608
35. Kandlikar SG (1998) Boiling heat transfer with binary mixture: Part-II, A theoretical modeling for pool boiling. National Heat Transfer Conference, Baltimore, Maryland, August 8–12
36. Suhas BG, Sathyabhama A Experimental investigation of heat transfer coeffient and correlation development for water-ethanol mixture in conventional channel. Journal of Thermal Science and Engineering Application, ASME. (Accepted), paper ID: TSEA-16-1089
37. Tsou MS, Fu BR, Pan C (2011) Critical heat flux on flow boiling of ethanol–water mixtures in a diverging microchannel with artificial cavities, 8th International Conference on Heat Transfer, Fluid Mechanics and Thermodynamics, 11 July – 13 July; Pointe Aux Piments, Mauritius